McGill Physical Journal

Measurement of Muon's Trajectory with Spark Chamber Detector

Alaina Bui

McGill University Department of Physics

11 Sept, 2017

PHYS 396: Research Project Final Report

Abstract

The spark chamber at McGill - an ionization particle detector used to analyze muons' trajectories - was recommissioned. Sparks were recorded with two cameras perpendicular to each other to obtain the true incident angles of the particles in three dimensions. The angular distributions of muons were found to approximately follow the currently accepted $\cos^2\theta$ model of the flux of muons [1]. Furthermore, different mixtures of argon and helium (respectively 0%:100%, 10%:90%, and 25%:75%) were used; there was a spark colour change from purple to blue, however no definite correlations were made between the change in gas composition and the chamber's efficiency due to low data collection and rather imprecise mixing of gases.

1 Introduction

Cosmic rays are fully ionized atomic nuclei and other particles accelerated from astrophysical sources that constantly cascade on Earth. The two types of cosmic rays are: primary, which are composed mainly of protons that collide with atoms and air molecules when they enter Earth's atmosphere; and secondary, which are created in these collisions and reach the Earth's surface [1]. These collisions produce a plethora of lighter particles, including pions (π^+, π^-, π^o) and kaons (K^+, K^-, K^o). While neutral pions (π^o) decay into photons and consequently form an electromagnetic cascade by creating more photons, protons, antiprotons, electrons, and positrons, the charged pions (π^+, π^-) decay into neutrinos and muons, as shown in Figure 1. Of the particles created in these showers, the most abundant at sea level are muons [2].

The muon is a particle that was first identified in cosmic ray experiments by Anderson and Neddermeyer in 1936. It is an elementary particle with an electric charge of -1 e and a spin of 1/2. Classified as a lepton, it is not believed to have any sub-structure (or to be composed of any simpler particles). Although the muon is an unstable subatomic particle with a mean lifetime of 2.2 μs, they are still able to reach and even penetrate the Earth's surface due to the fact that they travel near the speed of light and experience relativistic effects [3]. Since muons actually reach sea level and are relatively easy to detect, their angular distribution is observed using ionization particle detectors - in this case, the spark chamber.

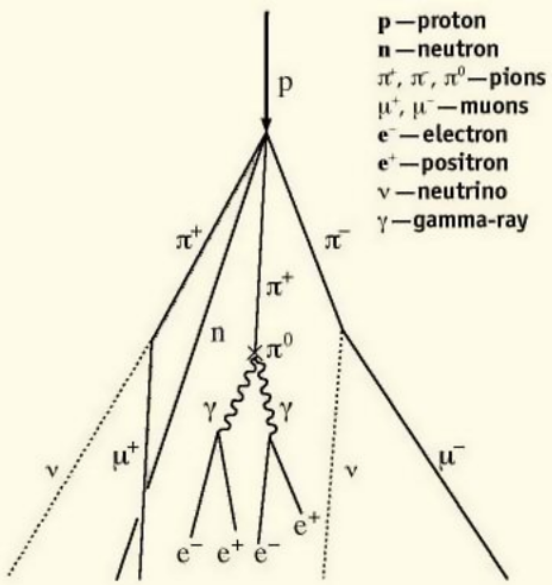

Figure 1: Some of the lighter particles that are produced when protons collide with air molecules in the upper atmosphere. Several particles - like kaons - are not displayed, but are still a result of the interaction [4].

In 1949, J. Warren Keuffel first observed that a discharge between parallel plates occurred along the path of charged particles passing through. T. E. Cranshaw and J. F. De Beer used this concept in 1957 to introduce the idea of applying high voltage to the plates immediately

after the passage of the particle and leaving it off at all other times. They also developed the triggering system to do so, using a Geiger telescope which gives a coincidence pulse when a particle goes through the detector; this pulse, after going through a delay network, triggers a hydrogen thyratron which switches a high voltage pulse onto the detector [5]. This was then developed into a spark chamber, which is a stack of parallel plates in an enclosed transparent casing filled with gas, with every other plate charged to a high voltage and the rest to ground. As a charged particle traverses the detector, it leaves behind a trail of ionized gas that results in a discharge when high voltage is applied across the plates. A spark is thus observed at the locations where the particle passes through and are subsequently documented to analyze the particle's trajectory. Spark chambers were used mostly as research tools and then were superseded in the 1980's by other technologies such as drift chambers and silicon detectors, as they have better time and spatial resolution [5]. Spark chambers are now mainly used for demonstrations.

The spark chamber at McGill University was first built in the summer of 1996 under the supervision of Professor F. Corriveau. An acoustic data acquisition system was later developed, but in 2012 a new system as well as data analysis software were introduced, consisting of capturing on video the muons' trajectories as they pass through the detector.

Muons are the most numerous charged particle at sea level. Most are produced high in the atmosphere and lose about 2 GeV to ionization before reaching ground. The flux of muons at Earth's surface is approximately described by $I_o \cos^2 \phi$, where ϕ is the zenith angle and I_o is the flux at 0°, which is roughly 70 $\mathrm{m}^{-2}\ \mathrm{s}^{-1}\ \mathrm{sr}^{-1}$, where $[\mathrm{m}^{-2}\ \mathrm{s}^{-1}\ \mathrm{sr}^{-1}]$ is the unit for integral intensity. This experiment seeks to replicate and improve the data taking of the spark chamber as well as verify the $\cos^2 \phi$ distribution by reconstructing the trajectories in 3D as well as make modifications to the gas composition.

2 Experimental Setup

The spark chamber consists of 26 parallel metal plates, each held 1 cm apart by equally sized rubber stubs and held down by a weight to prevent the plates from warping upwards at the center. The plates are placed in an enclosure made of Plexiglass that is filled with 99.995%

helium gas. The encasing serves to keep gas in as well as dust out. Any dust that remains on the metal plates will result in a discharge occurring at that location, creating unwanted sparks.

To determine whether or not a particle has passed through the chamber, a trigger system was designed to read the output signals of two scintillators placed at the top and bottom of the chamber, demonstrated in Figure 2. These scintillator materials are made out of fluorescent plastic [6], which have the special property of spontaneously emitting energy when their atoms are excited. When a charged particle passes through the scintillators, photons are emitted and travel along a waveguide until they reach the photomultiplier tubes (PMT) - powered to 1900 V by a Tennelec TC-952 power supply - that use the photoelectric effect to convert the photons into electrons. This electric current is then amplified and the output is an analog signal, which is then passed to the discriminators.

Discriminators are logic modules that output a digital pulse from an analog signal; the one used in this experiment is the LeCroy octal discriminator of model 623B. The threshold on the signal is set to approximately 50 mV to reduce background noise, since the noise generated by the PMT's is below 30 mV. To make sure that the particles have passed through the chamber - or both scintillators - only coincidences between the signals coming from the PMT's are relevant. Therefore, the analog signal is sent into the logic unit: an AND gate that outputs a logical "1" when both inputs are "1" also; otherwise, it outputs a digital "0".

The coincidence pulse of "1" cannot, however, be used directly as a trigger to the high voltage, thus it is first sent to the spark driver amplifier. The spark driver amplifier is powered with a positive input voltage of 206 V. When the logical "1" is sent to the spark driver amplifier, it uses a positive high voltage of 6 kV to amplify the signal and send it to the spark gap. When the spark gap is triggered, a high voltage supply of 12 kV is applied to every other metal plate, with the rest of the plates grounded. Immediately after the high voltage is applied, a 110 V clearing field is applied to the spark gap circuit. Both the clearing field and the positive input voltage to the amplifier are powered by VWR 105 power supplies.

The accumulation of charge on the plates due to the large voltage discharges at the location of the ionized gas, therefore marking the location where the particle passes through.

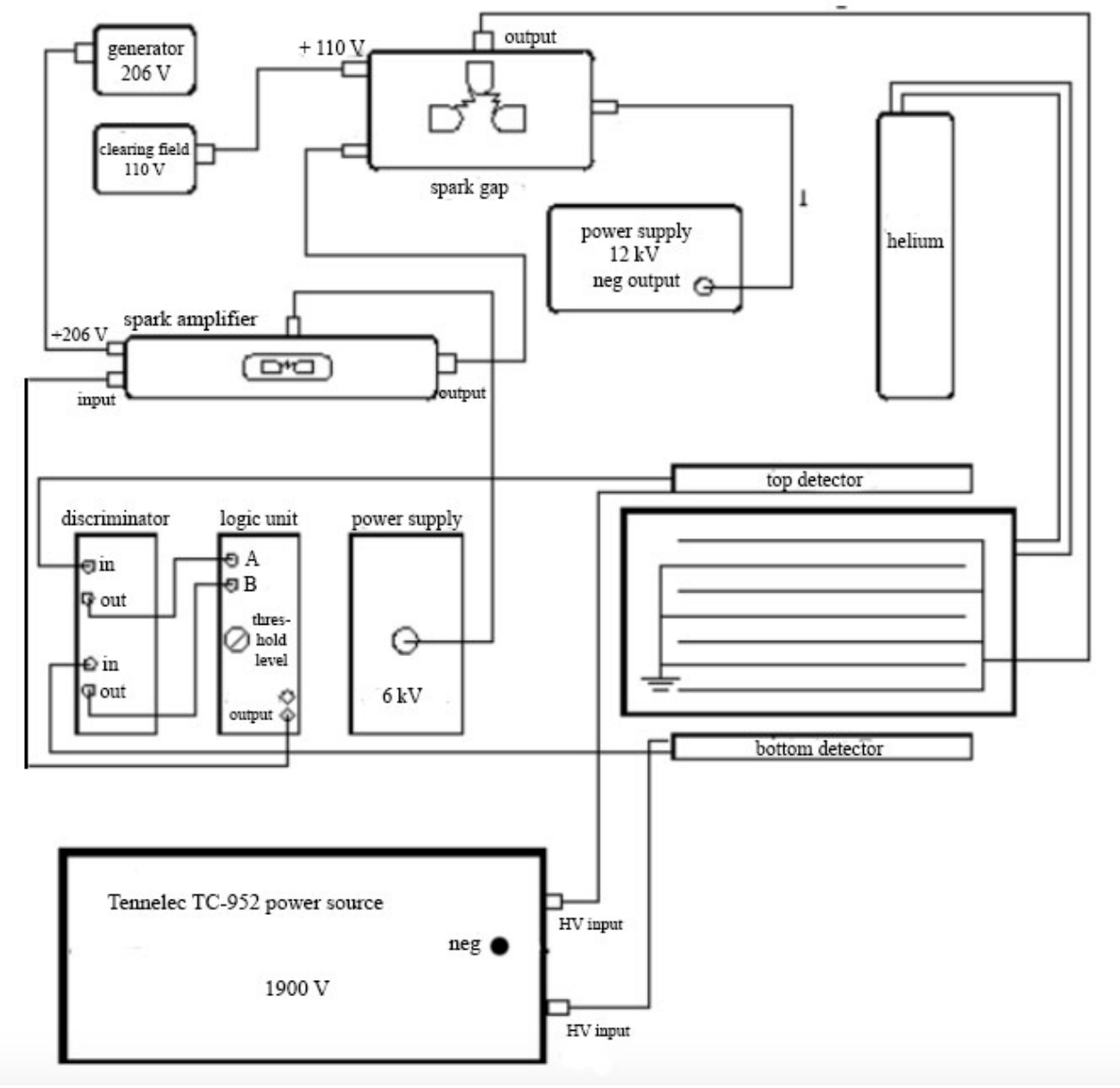

Figure 2: Diagram of the spark chamber's set-up [6]. Even though the top PMT requires 1800 V and the bottom 1900 V, 1900 V was supplied to both using one Tennelec power supply, as there is only one power source available and the 100 V difference does not have significant effects. The 206 V generator to the spark amplifier and the clearing field for the spark gap are both powered by VWR 105 power supplies.

The ejected electrons eventually recombine with the ions, with the rate of recombination determined by the gas. An electronegative gas such as oxygen recombines rapidly, while inert gases recombine more slowly. One of the noble gases is therefore employed; helium was chosen because it is relatively cheap compared to other noble gases. The choice of gas filling

is governed by several factors: low working voltage, high gain, good proportionality, and high rate capability [7]. These conditions are usually met by using a gas mixture; therefore, a 4.5 purity (99.995%) was chosen instead of a 5.0 (99.999%).

The recombination of the ionization charge of the helium between the plates is on the order of microseconds, while the time delay between a particle passing through the chamber and the application of the high voltage on the metal plates is on the order of several nanoseconds. Therefore, the helium is still ionized when the voltage is applied across the plates. The plates are not kept at high voltages at all times and are instead charged only when a particle is detected, because continuously applying high voltage across the plates results in noise due to the accumulation of charge on the plates. This consequently reduces the detection efficiency of the chamber. Charging the spark gap takes an amount of time that is on the order of milliseconds, so if a particle passes after the voltage has been applied but too soon for the spark gap to recharge, the particle will be missed. This time - the interval following successful sparking before the chamber can be used again - is called the dead time, which is estimated to be around 100 ms for spark chambers [8].

The supply pressure of the helium cylinder was set at 20 psi. The chamber was flushed for 4 hours before recording data at a rate of 150 standard cubic centimetre per minute (SCCM), and was turned down to 120 while data was being taken.

3 Data Acquisition

A new data acquisition system was introduced in 2012 by Jennifer Blanchard in place of the acoustic one, which consists of capturing images of the sparks to measure the angle of incidence of the particle. The sparks were filmed and later a program was written in MATLAB to extract every frame of the clip and return only those with sparks.

Four trials were performed at the start, where the plates were supplied voltages of 9 kV, 10 kV, 11 kV, and 12 kV, with the spark amplifier's supplied voltage correspondingly 4.5 kV, 5 kV, 5.5 kV, and 6 kV. The frequency of sparks at each trial were calculated by counting the number of sparks at a specific time interval and dividing it by the time interval (this takes into account multiple sparks at a time, despite most of them not being accepted for

later trajectory analysis). This is shown in Table 1. Since an applied voltage of 12 kV yields the most frequent sparks - which is, on average, a spark once every 4.57 seconds - the rest of data was taken at this voltage.

Voltage Applied vs. Frequency of Sparks				
Voltage (kV)	9	10	11	12
Time between sparks (s)	66	20	10.2	4.57

Table 1: Table of the voltage applied to the metal plates versus the average time between each spark. The number of sparks were counted during a fixed time interval, and was divided by the time interval to obtain these results.

The room has to be completely dark, hence sparks were recorded with lights off and during the night to minimize light sources coming through the windows. One set of data was taken while a camera was placed in front of the chamber (the xy-plane), and another set was taken with one camera in front and one on a side of the chamber (the xy- and zy-planes).

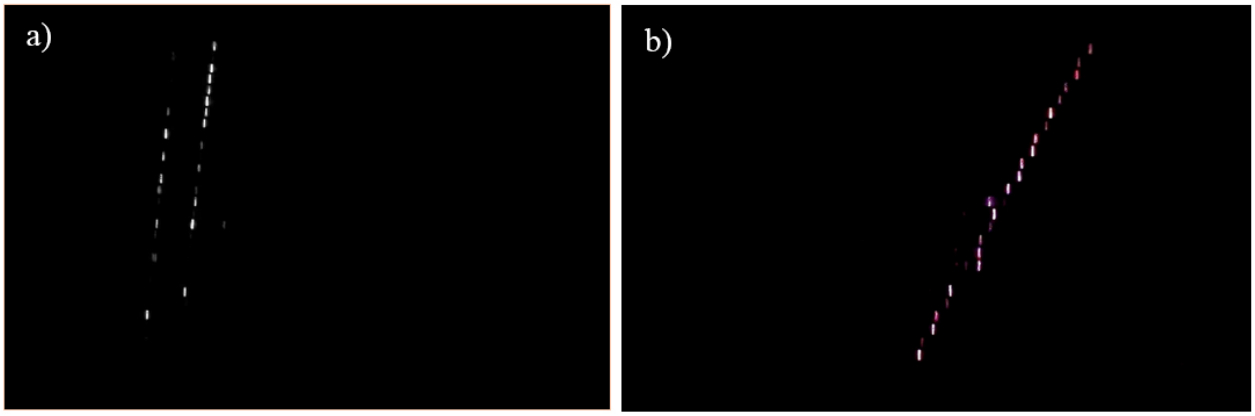

Figure 3: Part a) shows two sparks recorded on a frame in black and white and part b) shows a purple one before it is converted to black and white. As with most frames with multiple sparks, there are missing bright spots along the particle's path that makes it less convenient to analyze its trajectory; moreover, some overlap each other, making it hard for the program to separate individual sparks.

There were frames that have multiple tracks, which makes it more difficult to separate the sparks and analyze the trajectory of each particle; therefore, only frames with single tracks were accepted to analyze. To allow easier detection of sparks through MATLAB as well as reduce as much background noise as possible, images were converted to black and white. Moreover, there were sparks that span up to three frames; a program was written to combine

them, giving more data points to more accurately determine the particle's trajectory. Several examples are shown in Figures 3 and 4.

It was observed that sparks occurred first at the bottommost plates instead of the topmost ones (an example is shown in Figure 4, where the frame in part a) occurred before that in part b)). This could be due to the high voltage reaching the bottommost plates first, since the voltage applied is connected to the chamber at the bottom and the current has to travel along a wire to reach the top of the plate stack. Even though this takes a short amount of time, it is still enough to result in sparks materializing first at the bottom.

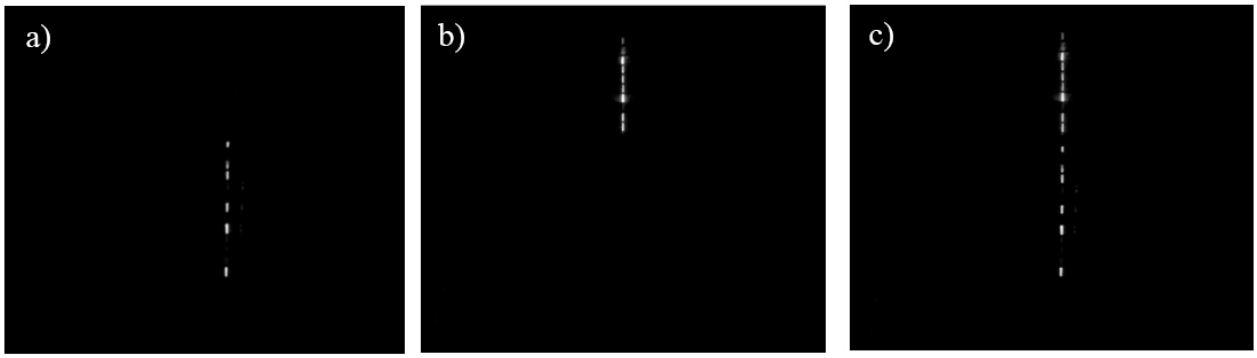

Figure 4: Parts a) and b) show the same spark that spans two frames, in the order that they appear. They were combined using Matlab to produce the image shown in c) to obtain as full a spark as possible.

4 Data Analysis

The data analysis process to find the incident angle from the particles' trajectories for both cameras / planes is similar. The coordinates of the bright spots were extracted from MATLAB and transferred to Python to replicate the particle's path. Any spurious sparks observed with the eye were removed from data. A linear fit was then applied to the data points using the method of least-squares; a linear model is possible since the muons do not curve as they pass through the chamber. Note: a magnet can be used in the experiment that curves the trajectory of the muon to determine its charge and momentum.

An example of a reconstructed track is shown, with residuals included, in Figure 5 up to scale of the original image (720 by 1080 pixels). A program in MATLAB extracts the midpoint of the bright spots as data points. The uncertainty was computed by finding the

distance between two ends of a bright spot, both vertically and horizontally. To determine whether or not the linear fit is sufficient, a chi-squared test was performed. If the null hypothesis - which assumes there is no linear relationship - is rejected, the fit is accepted and the angle of incidence is then extracted. The angle of incidence (θ) is computed by calculating the horizontal (dx) and vertical (dy) distances between two points on the linear fit, where $\theta = \arctan\left(\frac{dx}{dy}\right)$.

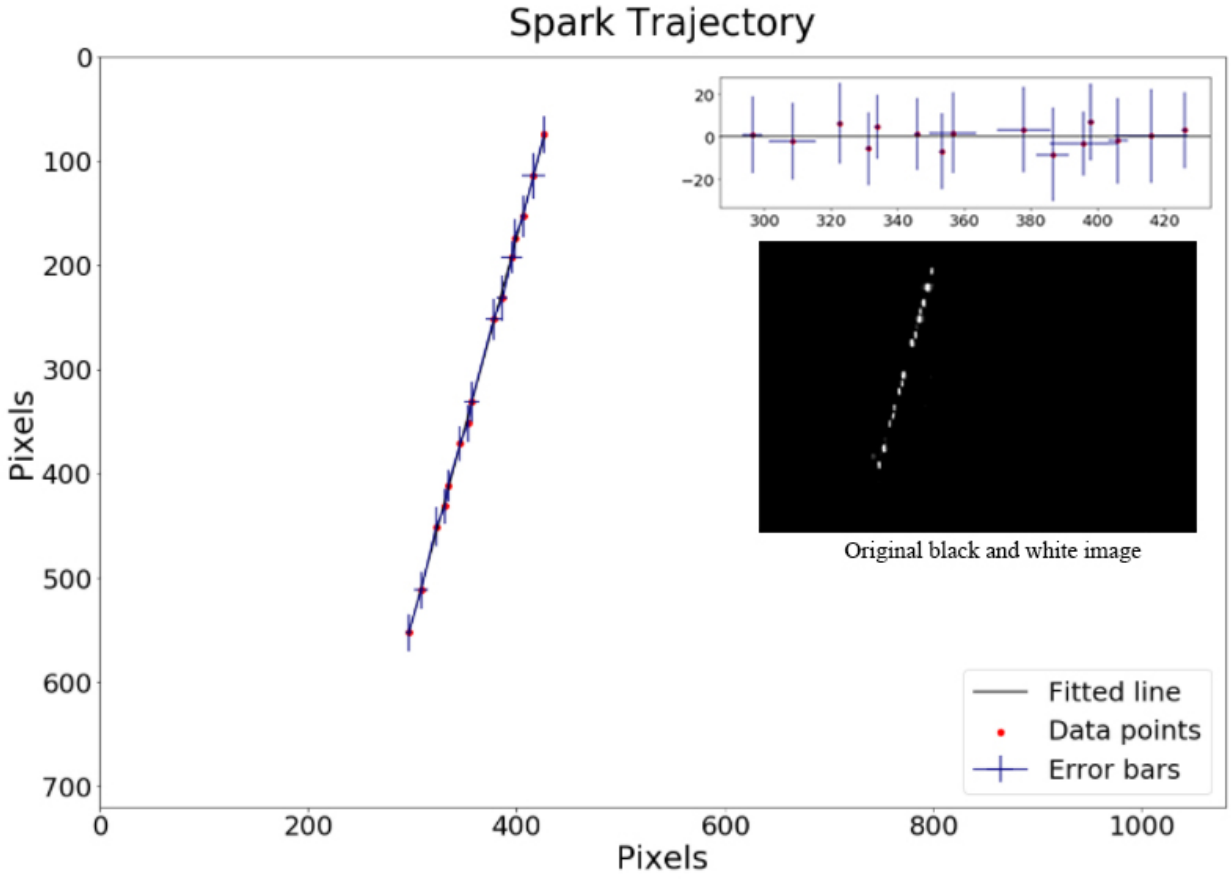

Figure 5: Spark trajectory constructed to scale of the original black and white image - included on the right - using Python. The residual is displayed at the top right corner and the legend at the bottom right. There are 15 data points, and hence 12 degrees of freedom (15 - 2 parameters - 1). The p-value calculated was 1.202, which is lower than the value on the chi-square distribution table: 21.03. The null hypothesis is thus rejected and the fit is accepted. Calculations were all made in Python.

Since the cameras were not perfectly aligned to the chamber and were instead slightly tilted, adjustments had to be made to the trajectory analysis in order to have the angles ascertained correctly. To obtain more accurate measurements, all spark trajectories for the

run with only one camera were rotated counterclockwise 1.1°; and those for two cameras in front of and on the side of the chamber were rotated counterclockwise 0.54° and 0.55°, respectively. These values were obtained by determining the coordinates of the four corners of the detector (points A, B, C, and D in Figure 6) and computing the angle at which the length along the detector can be perfectly aligned to the horizontal axis.

The acceptance of the detector also has to be accounted for. The dimensions of the plate stack are 25 cm wide, 66 cm long, and 35 cm tall. Due to the geometry of the detector, particles are more likely to be recorded if their angles of incidence are nearer to 0° than 90°. For example, particles that come at an angle θ are not observed by the detector along Δx. This applies also to the detector viewed along the zy-plane, where the width (W) is taken into consideration.

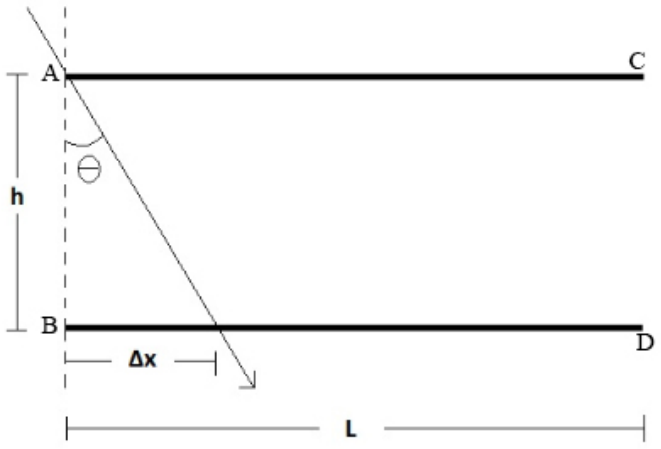

Figure 6: Sketch of the detector viewed from the xy-plane [9]. L is the length of the plates, h is the distance between the top and bottom plates, θ is the angle of incidence of the muon, and Δx is the loss in length L along the plate that a particle will be detected. Points A, B, C, and D are the corners of the detector.

The acceptance (A) of the detector is shown below, showing that the acceptance is 1 at vertical and goes to zero as the angle approaches 90°.

$$A_{xy} = \frac{L - \Delta x}{L} = 1 - \frac{h \cdot \tan\theta}{L} = 1 - 0.54 \tan\theta. \tag{1}$$

By determining the acceptance of the detector, events that could not be detected but are still present can be corrected for. This is done by dividing the data (number of events) by the acceptance.

5 Results and Discussion

5.1 2D Reconstructed Sparks

A camera was placed in front of the chamber and set to film. The maximum angle at which sparks could be measured in the xy-plane was also calculated to be $\theta_{max} = 62°$. This was done by measuring the length of the plates as well as the height of the plate stack, which were determined to be 66 and 35 cm, respectively.

$$\theta_{max} = \arctan\left(\frac{\text{length of plates}}{\text{height of plate stack}}\right) = \arctan\left(\frac{66\text{ cm}}{35\text{ cm}}\right) = 62°. \tag{2}$$

Moreover, it must be taken into consideration that sparks were viewed in only one plane. The true angle of incidence (ϕ) of the particle's path is projected along the plane of the front of the chamber - denoted θ_{xy} in this case. The $\cos^2\phi$ model thus does not apply to the angles measured and the relation between the true incident angle ϕ and the projected incident angle θ is described by equation 3, where β is the polar angle in the Cartesian coordinate system demonstrated in Figure 7.

$$\theta = \arctan\left(\tan\left(\beta\right)\cos\left(\phi\right)\right) \tag{3}$$

With the equation above, a Monte-Carlo simulation is subsequently introduced. The Monte-Carlo method builds models of possible results by sampling values at random from input probability distributions. The Monte-Carlo simulation in this case was generated by sampling possible values for the angles ϕ and β, where ϕ ranges from 0° to 90° and β ranges from 0° to 360°, since the particles arrive from random directions. After simulating the possible outcomes for ϕ and β, the distribution of the projected angle of incidence along the xy-plane $\theta_{xy}$was obtained. A sample, generated by a previous student working on the project using 3191 events, is displayed in Figure 8. The result can be compared to this model.

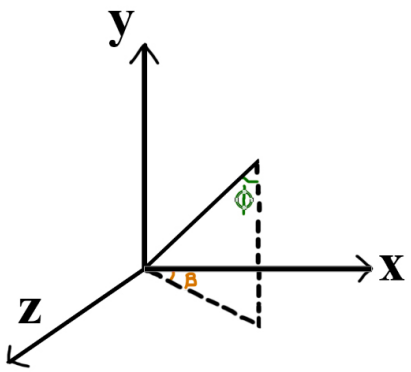

Figure 7: Definition of the angles ϕ and β in the xyz plane. ϕ is the true incident angle of the particles, and β is the polar angle. When viewed from only one plane - either xy or zy - the angle ϕ is projected onto said plane.

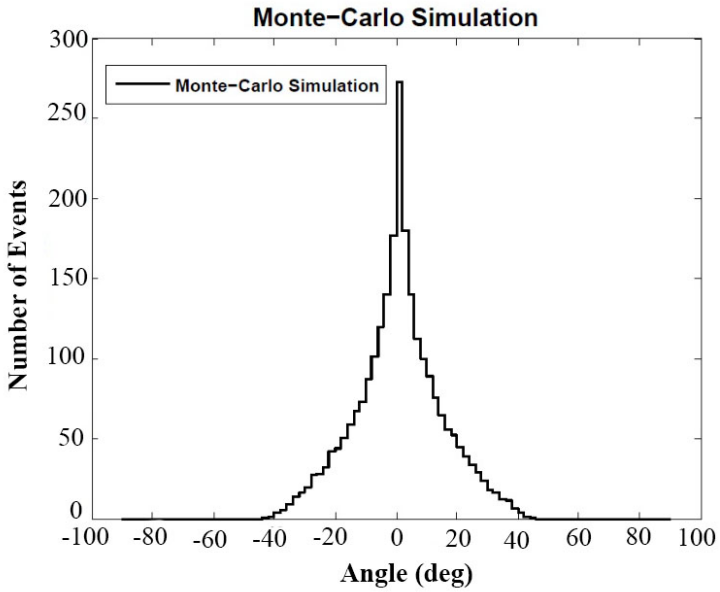

Figure 8: Monte-Carlo simulation of the $\cos^2\theta$ distribution, developed by a previous student working on the spark chamber [9]. There were 3191 events analyzed, hence the peak reaches almost 300 events.

A problem of having the negative end of the angular distribution overshooting the model was encountered in a previous experiment, which raised the possibility that the scintillators triggered more often when a particle passes near the readout side into the PMT's. Therefore, to increase efficiency in this experiment, the scintillators coupled with the PMT's were rotated 180° both on top and at the bottom of the chamber for half of the data collection procedure.

The angular distribution of the sparks projected along the front of the chamber is shown in Figure 9 with a total of 800 events analyzed after being divided by the detector's acceptance. This is a relatively low amount of data; better measurements could be made with more data collection. The incident angles were placed in a histogram with bin widths of 2°. The data was assumed to be governed by a Poisson distribution. This is due to the fact that a Poisson distribution models the probability of a number of events occurring within a fixed interval of time and space if these events occur independently of the time since the last event, which works because the generation of muons through the chamber is random. The error on each bin is therefore $\alpha = \sqrt{N}$, where N is the number of events in that bin.

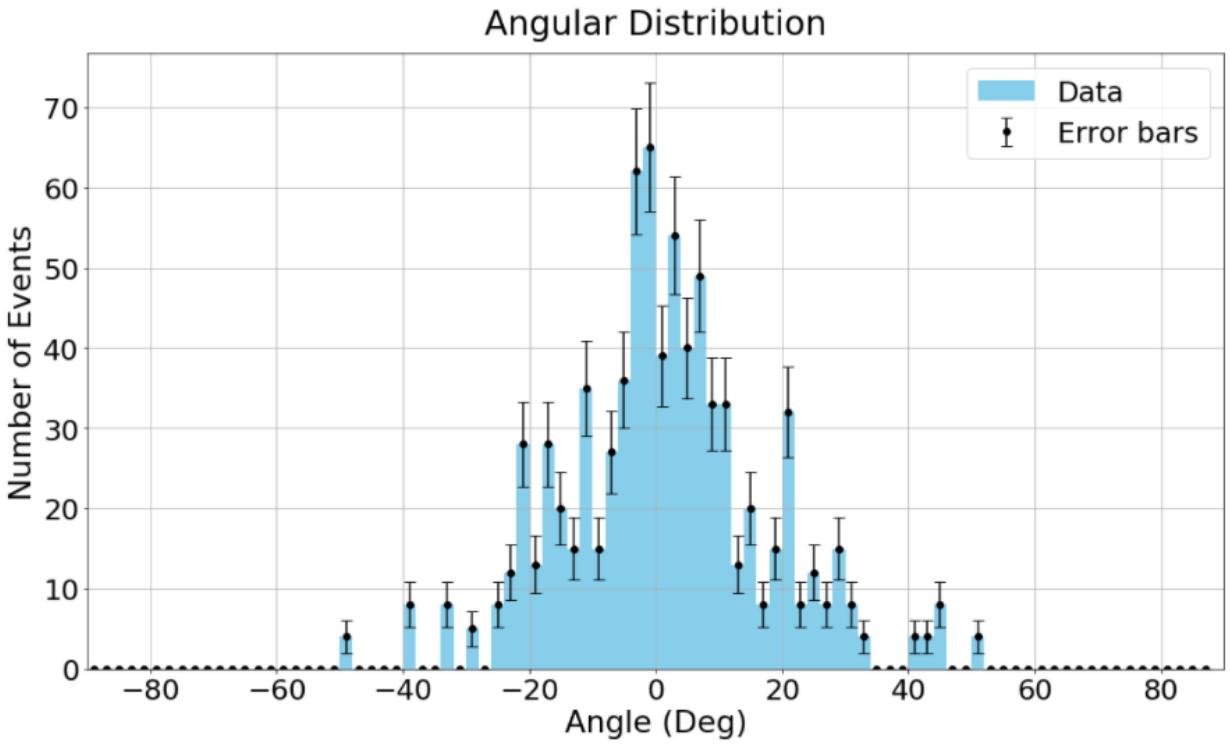

Figure 9: Angular distribution of the sparks along the xy-plane (θ_{xy}). The angles are measured in degrees. The peak is at 0°, agreeing with theory that particles most likely pass through the detector completely vertically.

The number of events measured in this experiment is 800, which is much fewer than the 3191 events in the Monte-Carlo sample in Figure 8, but their shapes are similar. There should be a peak at 0° with a symmetric distribution on both sides as well as no data after ± 62°, which is indeed the case in Figure 9, although interestingly there is a dip towards the positive angles near 0°. Overall, the measured angles roughly follow the Monte-Carlo sample of the $\cos^2\phi$ distribution.

5.2 3D Reconstructed Sparks

As mentioned in Section 1, the muon flux at Earth's surface is described by $I_o \cos^2(\phi)$, where I_o, the integrated flux, is approximately 70 m^{-2} s^{-1} sr^{-1} at sea level, which increases as the height at which the muons are detected increases. This is demonstrated in Figure 11, where a $\cos^2\phi$ distribution is displayed. The actual number of events recorded, however, does not precisely follow this $\cos^2\phi$ relation. Demonstrated in Figure 10, the number of recorded

muons are low at 0°, steeply peaks towards 10°, and gradually falls to 0 as the incident angle to the zenith increases. This is because, at 0°, the area through which the number of muons are detected is small, and thus the integral intensity should be low. As the zenith angle increases, there is a larger area through which the muons can be detected; therefore, the number of events quickly peaks at smaller angles and then decreases at larger angles.

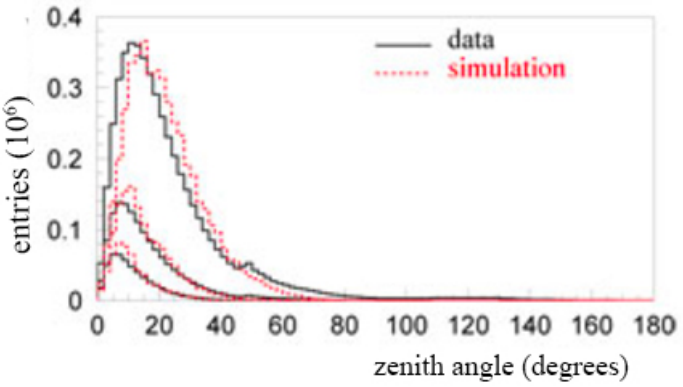

Figure 10: Zenith angle distribution of reconstruction tracks of data as well as simulated muons [10].

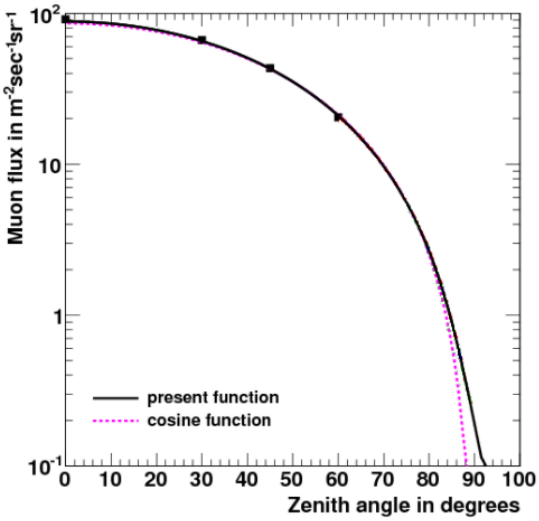

Figure 11: Muon flux as a function of zenith angle at sea level [11].

Two cameras were placed to film in front of and on one side of the chamber in order to analyze the sparks in three dimensions. The projected angles of incidence were measured from both cameras in the same fashion as before, only this time the acceptance of the detector for the angles recorded on the side of the chamber was calculated to be $A_{zy} = 1 - 1.4\tan\theta$. The maximum angle at which a particle could be detected is one that traverses diagonally across the detector: $\phi_{max} = 64°$. The true angle of incidence, ϕ, was determined through equation 4, where θ_{zy} is the projected angle along the zy plane (side of chamber) and θ_{xy} is the projected angle along the xy plane.

$$\phi = \arctan\left(\sqrt{tan^2(\theta_{zy}) + tan^2(\theta_{xy})}\right). \tag{4}$$

The angular distribution is only evaluated at positive angles because only the positive angles can be ascertained in three dimensions regarding the incident angles of the particles.

Since the angles were measured from two cameras instead of one this time, the error on the content of the bins is computed to be $\alpha = \sqrt{2N}$. The angular distribution of the sparks in three dimensions is shown in Figure 12, with 293 events analyzed.

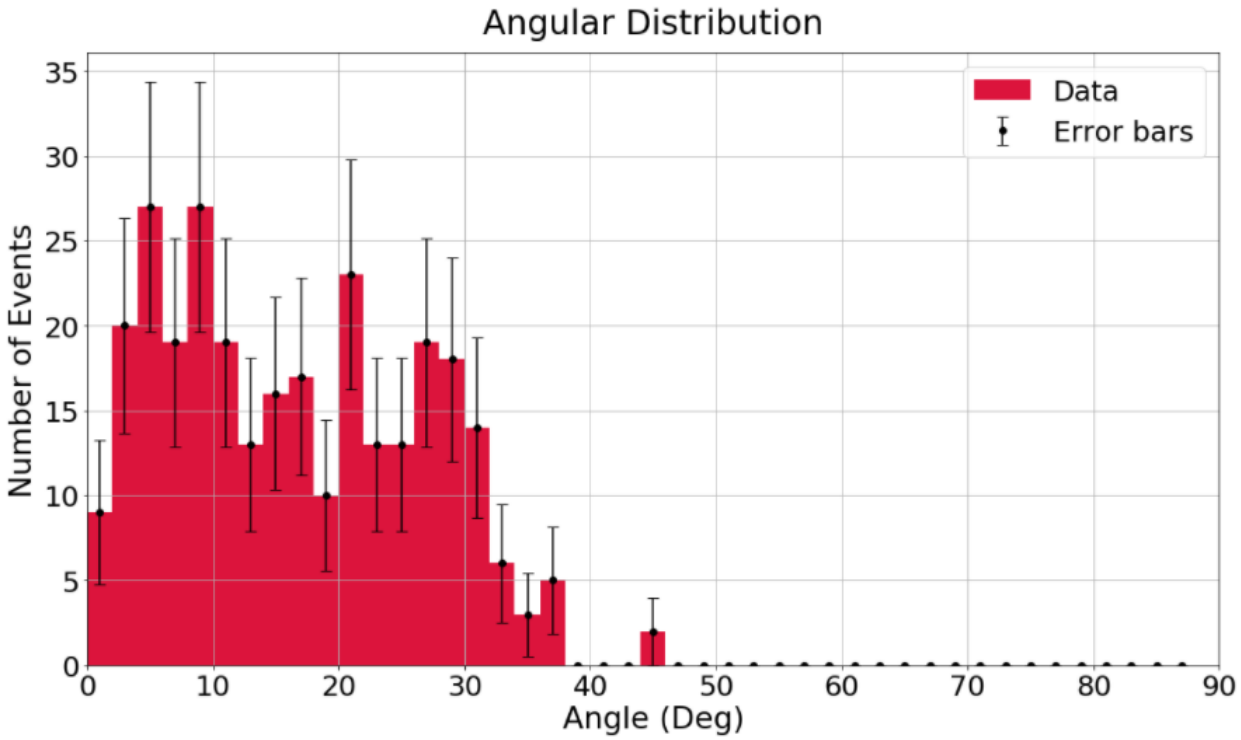

Figure 12: Angular distribution of the sparks in three dimensions, which roughly follows a $\cos^2\phi$ relation. Only positive angles are needed to determine the incident angles of muons, thus only the angular range from 0° to 90° is shown.

There are few events near 0°, which increases and then gradually decreases as the incident angle ϕ grows larger. This distribution is similar to that in Figure 10, which peaks around 10° and are very few at zenith angles larger than 50°. The muon angular distribution obtained approximately observes a $\cos^2\phi$ relation, which is characteristic of muons with energies of around 3 GeV [1].

The data also reflects the energy loss that muons experience: more muons pass through the detector when they travel vertically than at an angle. As for muons approaching from more horizontal directions, the intensity is naturally reduced because of muon decays and absorption effects in the thicker atmosphere at large zenith angles. Because of this, measurements of almost horizontal muons is difficult. Due to the geometry of the spark chamber detector, no particles coming horizontally - at a zenith angle of 90° - could be detected.

Adjustments to the detector to account for horizontal muons could be possible for future developments of the spark chamber at McGill.

5.3 Argon and Helium Mix

One of the primary factors affecting the performance of a spark chamber is the gas composition. Noble gases have a high affinity for electrons, making them ideal for the chamber. Helium was used because it was relatively cheap compared to other noble gases. However, adding a small quantity of argon (approximately 1%) to helium may improve the chamber's efficiency [1]. This is because argon has a relatively low ionization energy compared to helium, thus its atoms can be ionized by colliding with excited helium atoms which are in a metastable state energetically higher than the ionization energy of argon [1]. Adding argon to helium can result in extra electrons made in the avalanche, thus yielding higher efficiency.

An argon bottle was added to mix with helium. It was connected to a different flow meter, and the output of the flow meter was joined in with the helium output using a T-connector and subsequently flushed into the chamber. The units of the flow meters are in SCCM, and range from 0 to 150. To ascertain the amount of argon and helium in the chamber, the mass flow ratio between the two gases must be taken into account. Equation 5 was used to calculate mass flow, where $\dot{m}$ is mass flow, ρ gas density, $\dot{V}$ volumetric flow rate, m mass, and V volume determined from the ideal gas law.

$$\dot{m} = \rho \cdot \dot{V} = \frac{m}{V} \cdot \dot{V} = \frac{mP}{nRT} \cdot \dot{V} \tag{5}$$

The only two factors that can be adjusted are the outlet pressure of the gases and the volumetric flow rate. Since the flow meter only reaches 150 SCCM, it is difficult to precisely mix 1% of argon into helium. The chamber was therefore flushed first with only helium for 4 hours, 25% argon with 75% helium for one hour, and 10% argon with 90% helium for another hour. A Nikon D90 camera was used to record the sparks at an exposure of 4 seconds - since there is, on average, a spark every 4.6 seconds. The exposure and aperture values were kept fixed for the entire duration, as well as the applied voltage at 12 kV.

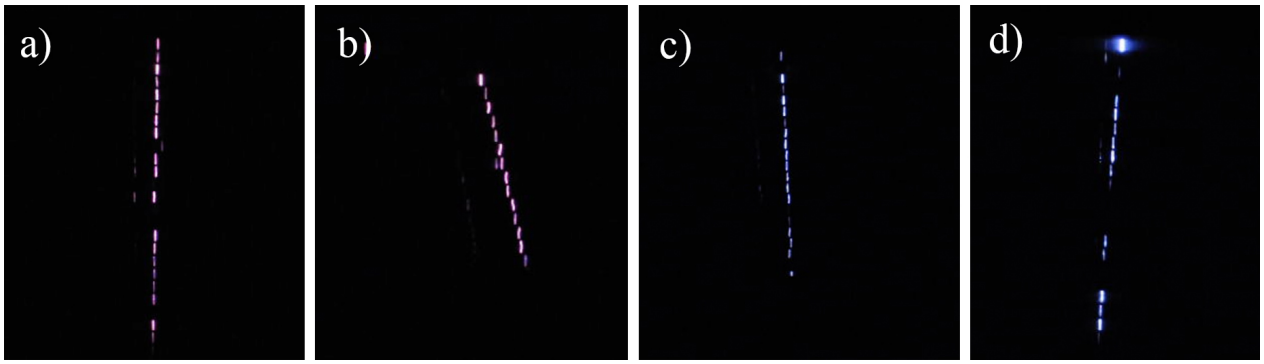

Figure 13: Part a) shows that the sparks are blue when there is 25% argon, while part b) shows that the sparks are purple when the chamber is flushed with only helium.

While neon produces red sparks and helium produces purple ones [1], a mixture of helium and argon gives blue sparks, demonstrated in Figure 13. For a helium-only chamber, there was a spark once every 3.9 seconds; for a mixture of 25% argon, sparks were observed every 3.9 seconds; for 10% argon, it was every 3.6 seconds. Since the videos were recorded for merely five minutes due to the restricted time allowance of the camera, no repeated measurements were made, and the chamber was not flushed consistently for 4 hours for each mixture, no correlations were made as to the effect the mixture of argon and helium had on the frequency of sparks. This could be replicated and improved in a future project to reach better conclusions.

6 Conclusion

The spark chamber at McGill have undergone various adjustments to maintain and improve it. In this project, changes were made to the spark chamber through measuring the true angle of incident by viewing the sparks from two planes, as well as experiment with a mixture of argon and helium gases. The $\cos^2\theta$ model was confirmed for the flux of muons, as the measured angles approximately follow the distribution. There were no certain verifications that adding argon made changes to the detector's efficiency, since the sparks were recorded at a short amount of time and the chamber was not properly flushed for at least 4 hours each time. The only noticeable change was that the colour of the sparks turned from purple to blue.

For a future project, it could be a good idea to observe the effect that different mixtures of noble gases could do to the chamber's efficiency, although this could be cost-inefficient. A higher amount of data collection would also be helpful to more accurately and precisely compare the results to currently accepted models.

Sine the chamber had been used for many years, a Plexiglas or acrylic aquarium could also be used in place of it. It would be possible to remove the top of an aquarium, flip it, and insert a tube for gas to flow from the bottom to reach the top of the aquarium in order for helium to be flushed from the top down. This way there will not have to be holes drilled into the aquarium.

References

[1] J. M. J.J. Beatty and S. Wakely, "Cosmic rays," *Particle Data Group*, pp. 4–7, February 2012. 1, 14, 15, 16

[2] P. Karn and C. Kearsley, "Measuring the angular distribution of cosmic ray muons," *Phillip Dudero*. [Online]. Available: http://mxp.physics.umn.edu/s07/projects/s07_cosmicraysdistribution/Default.asp 1

[3] B. Martin and G. Shaw, "Particle physics," *John Wiley and Sons Ltd*, pp. 279–288, 2008. 1

[4] G. A. Williamson, "Cosmic ray conversions," *Glen A. Williamson*, 2015. [Online]. Available: http://www.williamson-labs.com/cbr-tech.htm 1

[5] S. A. Bull, "What is a spark chamber?" *University of Birmingham*, September 2001. [Online]. Available: http://www.ep.ph.bham.ac.uk/general/outreach/SparkChamber/text1hh.html 2

[6] A. Robichaud-Véronneau and F. Corriveau, "Spark chamber," *Andrée Robichaud-Véronneau*, October 1999. 3, 4

[7] W. R. Leo, "Techniques for nuclear and particle physics experiments: A how-to approach," *Springer-Verlag*, pp. 140–144, 1987. 5

[8] W. Frass, "Particle detectors," *Oxford Physics*, 2009. [Online]. Available: http://www2.physics.ox.ac.uk/sites/default/files/Detectors.pdf 5

[9] J. Blanchard, "A measurement of angular distribution of cosmic muons," *McGill University*, August 2012. 9, 11

[10] A. A. et al., "First year performance of the icecube neutrino telescope: Muon track reconstruction," *IceCube Collaboratory*, pp. 21–22, May 2006. 13

[11] P. Shukla, "Energy and angular distributions of atmospheric muons at the earth," *Nuclear Physics Division, Bhabha Atomic Research Centre, Mumbai 400085*, pp. 5–11, June 2016. 13

Acknowledgements :

I would like to thank Prof. Thomas Brunner and Prof. Francois Corriveau for taking me on with this project. I would also like to thank Thanh Nguyen and Thomas Rosin for their help with the setup and data analysis along this project.

A Appendix

Figure 14: The spark chamber as viewed from one side (the zy-plane). The scintillators coupled with PMT's are above and below the chamber, and the electronics are at the bottom of the cart. The spark chamber is placed near windows as to let helium out of the room.

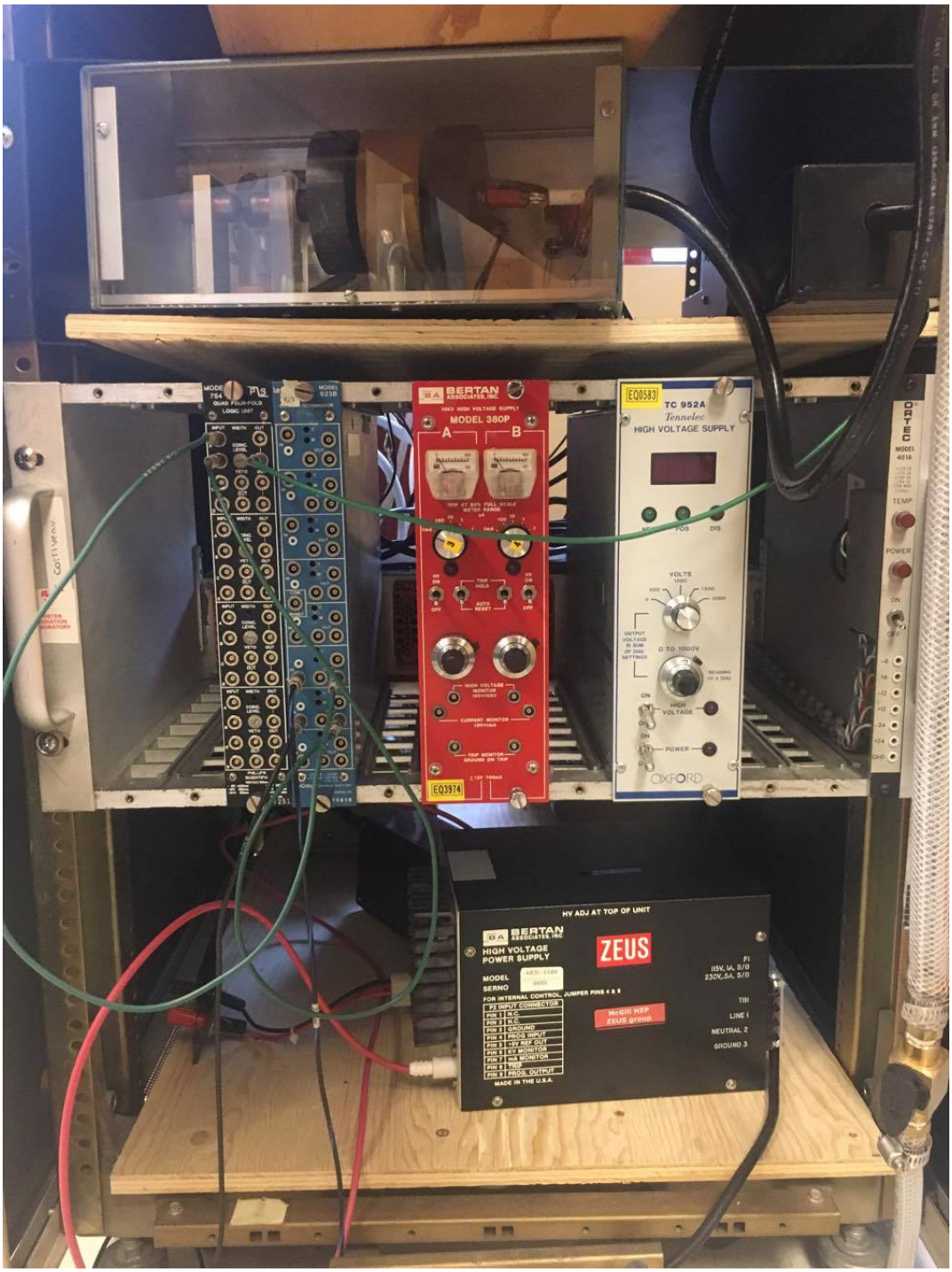

Figure 15: Below one side of the chamber. The spark gap is seen at the top, connected to the high voltage supply (Bertan, model 603C-150N) at the bottom to supply 12 kV to alternating metal plates. The Bertan model 380P red power supply supplies voltage to the spark driver amplifier. The white Tennelec TC-952 power supply supplies 1900 V to the PMT's. The signals from the PMT's goes into the blue LeCroy octal discriminator of model 623B, and is then sent to the black four-fold logic unit model 754. The NIM crate supplies power to the logic unit, discriminator, and the red power supply for the spark driver amplifier.

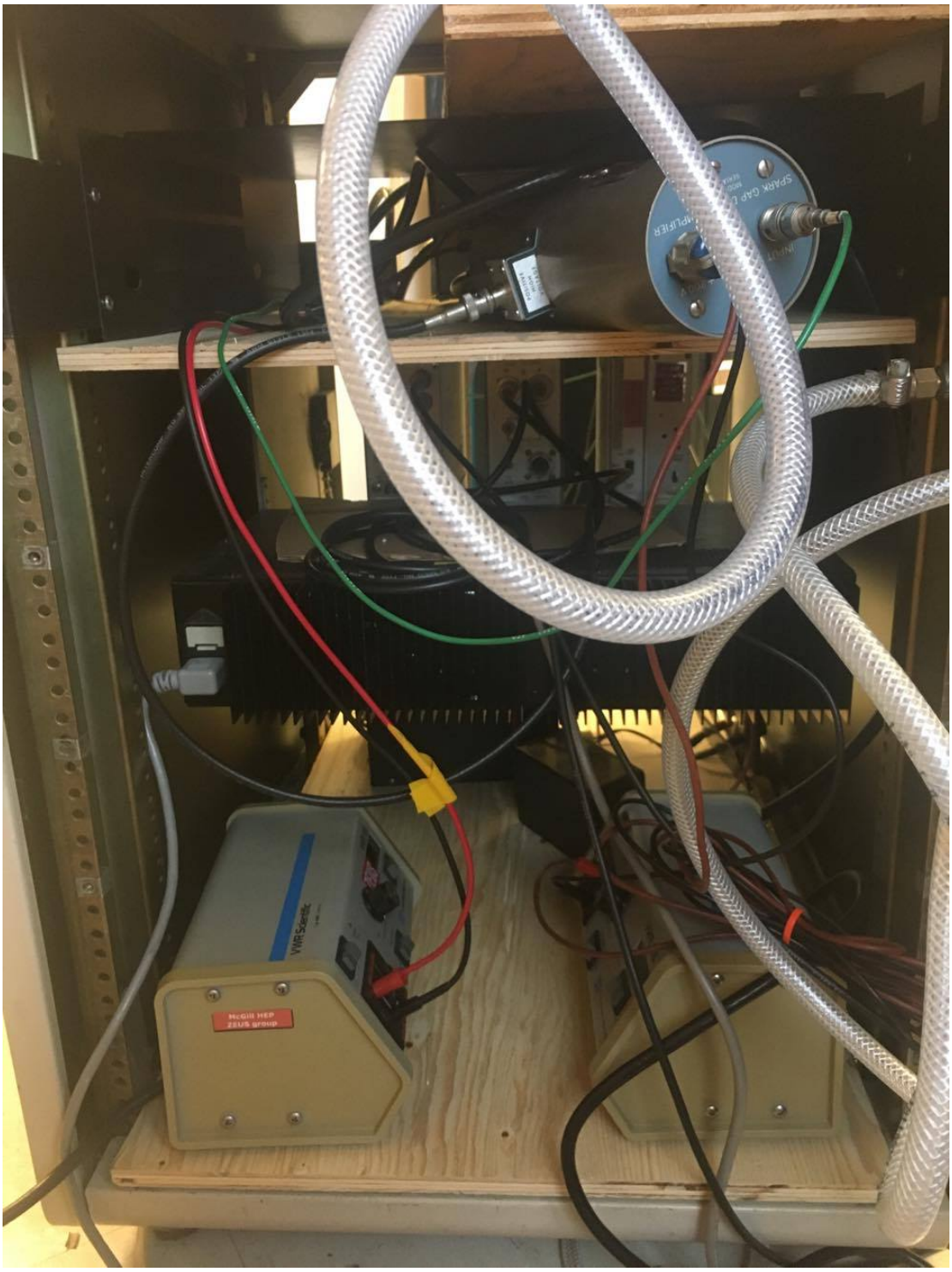

Figure 16: Below the other side of the chamber. The spark driver amplifier is at the top; sparks can be seen and heard from an opening in the middle. It is connected to a VWR 105 power supply (right) - the same power supply that generates a 110 V clearing field to the spark gap (left).

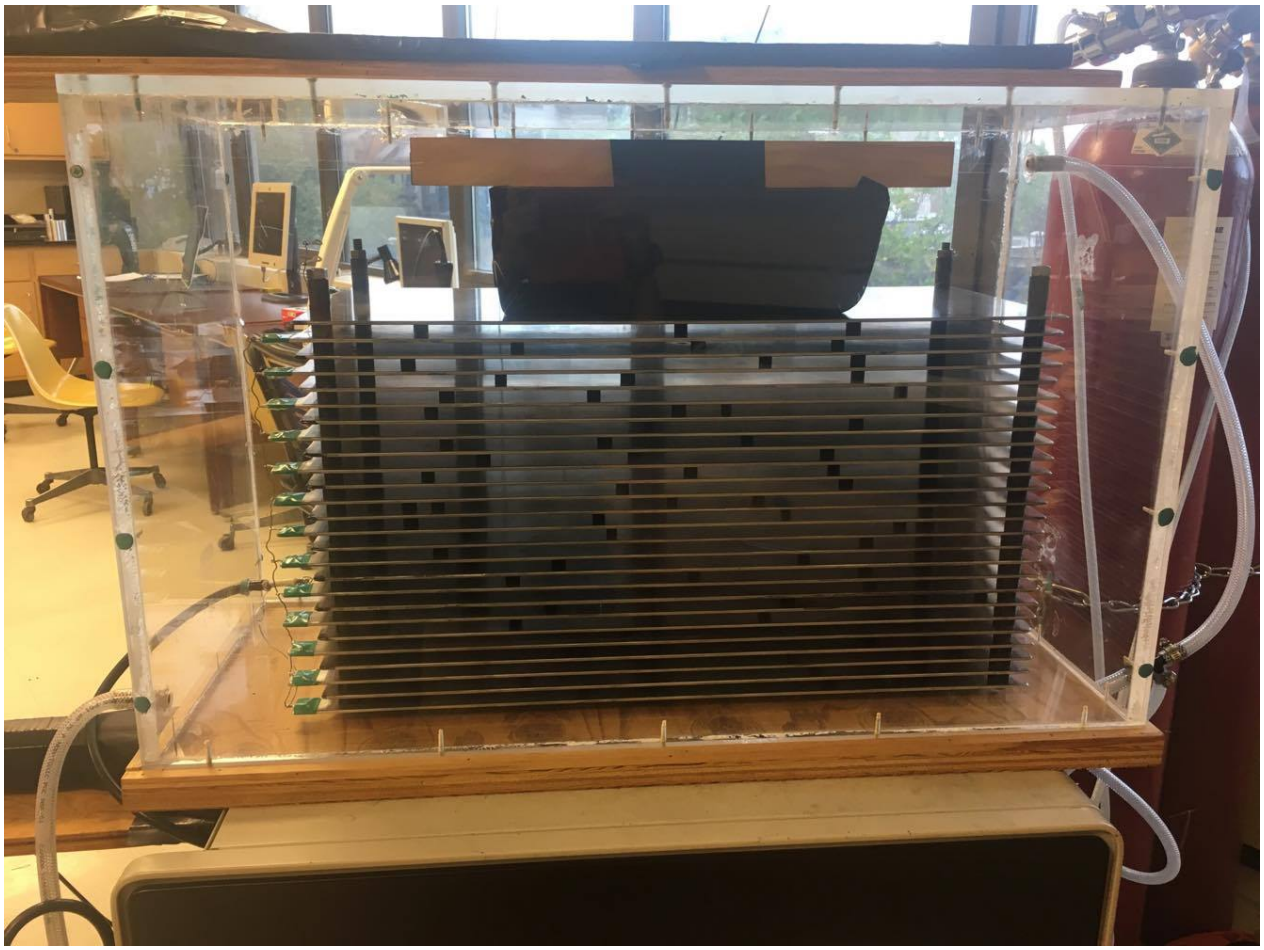

Figure 17: The spark chamber as viewed at the front (in the xy-plane). The 26 parallel metal plates are held down by a weight to prevent them from warping upwards at the centre. The red helium bottle is behind the chamber, attached to a pressure regulator and a flowmeter to flush the chamber with helium. The argon bottle, not shown, is next to the helium bottle.